Application of Finlets for Trailing Edge Noise Reduction of a NACA 0012 Airfoil

Felix Gstrein*, Bin Zang† and Mahdi Azarpeyvand‡
Faculty of Engineering, University of Bristol, United Kingdom, BS8 1TR

The present experiments investigate the reduction of trailing edge noise of a symmetric NACA 0012 airfoil using surface treatments, known as finlets. Treatment effectiveness is measured with observations from far-field data. Moreover, the highly instrumented airfoil model allows measurements of both static and dynamic surface pressure at various chord- and spanwise locations. In particular, measurements were carried out in between of the finlets, in order to elucidate clearly the near-field dynamics. With this, key parameters associated with trailing edge noise reduction could be identified. Relevant factors are, for instance, the spacing and the height of the finlets, as well as their relative positions with reference to the trailing edge. The results suggest that there possibly exists a strong correlation between the finlet height and the boundary layer thickness at the trailing edge. Attempting to identify different noise reduction mechanisms described in the previous studies, it was concluded that the prevailing one for airfoils is likely to be the detachment of small-scale turbulence structures from the airfoil surface. From the results of a position study it was inferred that shifting a treatment upstream from the airfoil trailing edge leads to beneficial effects in terms of trailing edge noise reduction compared to the configuration with the treatment applied flush with the trailing edge.

I. Nomenclature

c	=	airfoil chord length
l	=	airfoil span length
d	=	pinhole diameter
h	=	nozzle height
h_F	=	finlet height
l_F	=	finlet length
p_F	=	finlet position
s_F	=	finlet spacing
C_p	=	pressure coefficient
f	=	frequency
p_0	=	reference pressure
p_{rms}	=	root-mean-square of pressure fluctuations
U_∞	=	flow speed
U_e	=	free-stream velocity
u	=	velocity distribution in x-direction
(x, y, z)	=	coordinate system set at the airfoil leading edge
(x_F, y_F, z_F)	=	coordinate system set at the finlet leading edge
α	=	geometric angle of attack
α_f	=	effective angle of attack
δ	=	boundary layer thickness
η, σ	=	angle of attack correction factors
Λ_z	=	spanwise correlation length
Φ_{pp}	=	power spectral density of the surface pressure fluctuations

*PhD Researcher, Mechanical Engineering, felix.gstrein@bristol.ac.uk.
†Research Associate, Aerospace Engineering, nick.zang@bristol.ac.uk.
‡Professor of Aerodynamics and Aeroacoustics, m.azarpeyvand@bristol.ac.uk.

II. Introduction

Noise radiated by flow-immersed objects has become an increasing public concern since high bypass ratio turbofans were integrated into aircraft propulsion systems in the 1970s [1–3]. Recent studies on the health risk of exposure to aircraft or industrial wind turbine noise, such as [4] or [5] respectively, emphasize the need for further efforts into more efficient noise reduction techniques. Considering an aircraft flying with retracted landing gear and flaps, trailing edge noise from the lifting surfaces was identified as the prevailing noise source by Lockard and Lilley [6]. For airfoils under such operating conditions, the noise is a direct consequence of the fluid-structure interaction with the sharp leading edge in the turbulent boundary layer. The present study is concerned with the application of surface treatments, known as finlets, to manipulate the flow characteristics in a turbulent boundary layer on an airfoil. In doing so, the aim is to achieve trailing edge noise reduction.

The fundamental mathematical description of the trailing edge noise of an flow-immersed object was formulated by Amiet [7, 8]. According to his seminal work, the far-field sound pressure power spectral density on the center line of a semi-infinite airfoil is a function of the surface pressure fluctuation power spectral density, Φ_{pp}, and the spanwise correlation length of turbulent structures, Λ_z. These quantities are functions of the frequency f and position-dependent. In other words, the near-field flow characteristics at the trailing edge are important contributors to the generation of trailing edge noise. Later, Roger and Moreau [9] modified the formulation by taking the leading edge back-scattering into account. Significant efforts have since been expended to design both passive and active noise mitigation strategies through manipulation of the boundary layer characteristics. Different approaches include trailing edge serrations [10–13], boundary layer suction and blowing [14, 15], porous trailing edges [16–18], morphing [19, 20], three-dimensional finlets [21] and trailing edge brushes [22].

The concept of finlets can be traced back to Lilley [23], reflecting on the functional principle of the downy surfaces found on the wings of silently flying owl species. Lilley established the theory that the fibers covering these surfaces dissipate the turbulent kinetic energy of the flow more rapidly than it would usually be dissipated through viscous effects. Later, Clark et al. [24] investigated the feathers of owl species and discovered that those fiber-built canopies were aligned in the flow direction. Subsequently, they designed fence structures termed finlets, which resembled the canopy structures on owl feathers [25]. Applying them on a DU96-W180 airfoil, they achieved as much as 10 dB broadband noise reduction. More interestingly, they further inferred from their flow measurements that, though originally tested at the trailing edge, finlets might show some additional benefits when shifted further upstream toward the leading edge. Afshari et al. [26, 27] applied similar finlets on a flat plate at various positions upstream of the trailing edge to examine the effects on near-field flow manipulation at the trailing edge. In doing so, two different noise reduction mechanisms were identified, depending primarily on the spanwise distance of the finlets to each other, i.e. the finlet spacing. When the finlet spacing was small, the flow acted similarly to a semi-permable backward facing step. On the other hand, beyond a certain spacing, a reduction of the surface pressure fluctuation power spectral density was achieved at frequencies from 1000 Hz to 10 000 Hz, whereas its level at lower frequencies remained more comparable to the untreated flat plate. The mechanism was referred to as "channeling", where an increase of friction is believed to lead to a higher dissipation rate of the turbulent structures in the boundary layer. More recently, Bodling and Sharma [28, 29] numerically studied finlets extending beyond the trailing edge of a NACA 0012 airfoil using a wall-resolved large eddy simulation (LES) approach. For the configuration considered, they attributed their noise reduction effects partly to the lifting of eddies away from the trailing edge.

Building upon the findings of previous work, the focus of the present study is to further extend the fundamental understanding of the noise reduction mechanisms by applying finlets on a symmetric NACA 0012 airfoil at a moderate Reynolds number. In particular, the highly instrumented airfoil model used allows measurements in between of the finlet walls, and thus to shed more light on near-field flow dynamics. Using a beamforming array, the far-field trailing edge noise of the airfoil was obtained with and without finlets. This helps to establish a connection between the near-field surface pressure fluctuations and the noise radiated into the far-field. The experimental set-up, inclusive of measurement techniques and parameters, is presented in Section III. To establish the near-to-far-field relation, the far-field data will be presented first in Section IV. This way, the most effective configurations can be identified. Subsequently, the near-field results for the selected treatments are presented and discussed in Section V. In particular, the results for the finlet treatments are divided into studies for finlet height, spacing and the effects of finlet position with respect to the trailing edge. In the discussion, the surface pressure fluctuation power spectral density Φ_{pp} and the spanwise correlation length Λ_z are related to the measured far-field noise. Concluding remarks and a preview on future work are given in Section VI.

III. Experimental Set-up

A. Finlet Design and Parameters

The finlet design for the experimental investigation on the NACA 0012 adheres closely to that of Afshari et al. [27]. Thus, it is possible to consistently relate and compare the present results with those associated with a flat plate. Figure 1 depicts the profile of the airfoil and the attached finlets as well as the relevant coordinate systems. A close-up view on the section of the airfoil prepared with treatments for one side is given in Fig. 2. As can be seen from Fig. 1, the NACA 0012 profile allowed for symmetric installation of finlets on both the pressure and suction side. The reference system consists of the chord- and spanwise direction x and z and the coordinate y normal to the airfoil center line. To facilitate the discussion, all parameters relevant to the finlet design are denoted using a local coordinate system, and labelled with a subscript F. The leading parts of the finlets are arched and extend from the surface similar to those used by Clark et al. [24], following the conventional thickness development of a turbulent boundary layer on a flat plate. The mathematical description for the finlet in the local coordinate system is

$$y_F = a \cdot x_F^{4/5}, \tag{1}$$

where x_F designates the streamwise coordinate axis, locally attached to the finlet leading edge and y_F describes the wall-normal direction. A parameter, a, was introduced to regulate the gradient of the arched front part. It was chosen such that the length of this section remains constant at approximately 33 mm. The rear part of the finlet is rounded with a radius equal to the profile height. The designed shape helps avoid sudden changes to the boundary layer. To

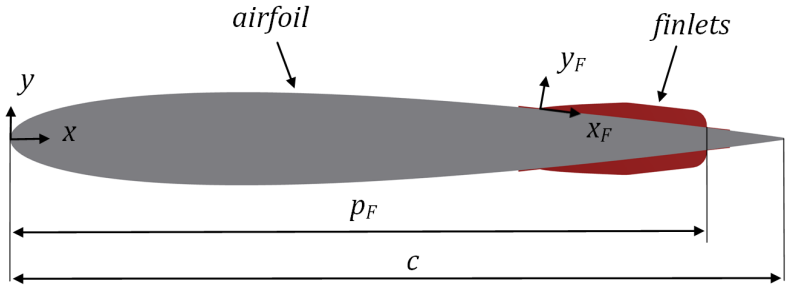

Fig. 1 Schematic of a NACA 0012 airfoil with a finlet treatment applied upstream of the trailing edge.

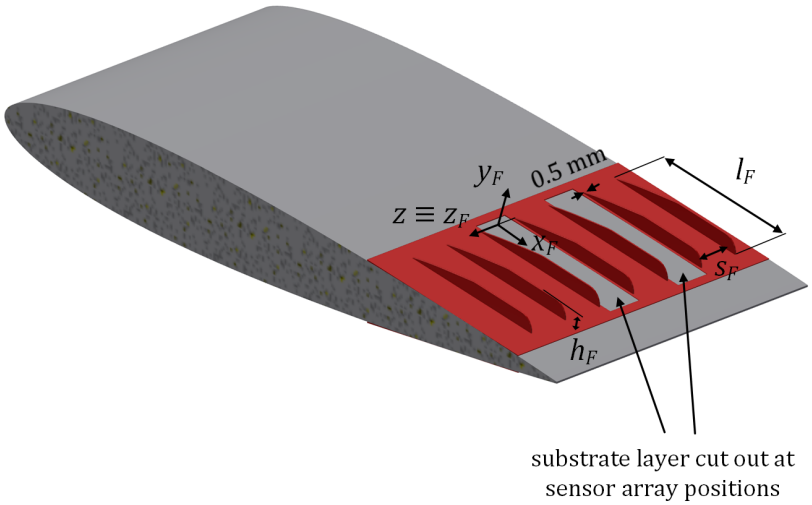

Fig. 2 Close-up view of a finlet treatment applied upstream of the airfoil trailing edge.

examine the effects of finlet geometry, different parameters such as the finlet height, h_F, length, l_F, and spacing, s_F, were considered in the experiment, as illustrated in Fig. 2. The treatment position, p_F, was defined as the distance from the airfoil leading edge to the finlet treatment trailing edge along the x axis, as shown in Fig. 1. The finlets themselves are 0.5 mm thick and supported by a flat, 0.3 mm substrate layer base. The position of the finlets was varied from $p_F = 0.63c$ to $p_F = 1.0c$ on both suction and pressure side. In this area, the curvature of the airfoil with chord c was sufficiently small to install a treatment without altering its flat base area. Moreover, in order to obtain the static and dynamic surface pressure measurements in between the walls of the finlets, the substrate base layer has been locally removed to uncover the pinholes for the sensors, as shown in Fig. 2.

B. Airfoil and Instrumentation

For the present study, the NACA 0012 model was chosen as the baseline. The airfoil model was produced from aluminium with a chord of $c = 300$ mm and a span of $l = 500$ mm. Two strips of 6 mm wide and 0.5 mm thick zig-zag turbulator tape were attached at $x/c = 0.1$ to trip flow into a turbulent boundary layer on both the suction and the pressure sides. In the present investigation, the airfoil is immersed into a uniform flow of approximately $U_\infty = 20$ m/s, which corresponds to a moderate Reynolds number based on the airfoil chord length of $Re_c = 4 \cdot 10^5$. The angle of attack, α, was adjusted such that for $\alpha = 0°$ the static pressure distributions on the suction and the pressure side were identical. The angle was then varied between $\alpha = 0°$ and $\alpha = 15°$ with the aid of turntables. Side walls were used to hold the airfoil model and to ensure two-dimensional flow along its span. As the airfoil was installed in an open-jet wind tunnel, the angle of attack had to be corrected to account for any changes to the pressure distribution due to flow deflection. Thus, the open wind tunnel correction for zero-camber airfoils proposed by Brooks [30] was applied. This correction has been employed by a number of studies under similar experimental conditions [16, 31, 32]. Following the same procedure as Brooks, the corrected angle of attack α_f was obtained as

$$\alpha_f = \frac{\alpha}{\eta}, \tag{2}$$

where

$$\eta = (1 + 2\sigma)^2 + \sqrt{12\sigma}, \tag{3}$$

and

$$\sigma = \frac{\pi^2}{48}\left(\frac{c}{h}\right)^2. \tag{4}$$

The parameter h designates the vertical stream width, which is equivalent to the nozzle height in the present case.

To capture a comprehensive set of static and dynamic pressure data, 48 miniature microphones and 64 pressure taps, distributed along both the chord and span of the airfoil, were employed for the measurements. Of the 48 miniature microphones, 32 were operated in a direct sensing configuration. For this, Knowles FG-23329-P16 condenser microphones were placed beneath pinholes of diameter $d = 0.4$ mm to reduce the sensing area and thus spectral surface pressure attenuation effects [33]. In areas where the airfoil thickness is too thin to accommodate in-situ pressure transducers (from $0.95c$ to the trailing edge), Panasonic WM-61A microphones were used in a remote sensing configuration. For these 16 pressure transducers, the dynamic pressure information is carried to the electronic device through polyurethane tubing. Readers are advised to refer to Elsahhar et al. [34] for more details on remote sensing. To determine the lateral correlation length of turbulence structures, an array of seven microphones, distributed along the airfoil span at $0.99c$, was used. A full description of the airfoil and its instrumentation can be found in [35] and [36].

C. Facility and Data Acquisition

All experiments were performed in the aeroacoustic facility of the University of Bristol, consisting of a temperature-controlled closed-circuit wind tunnel and an open-jet test section. The test section is fully anechoic above 160 Hz [37]. A nozzle with a cross-section of 500 mm in width and 775 mm in height is used to deliver a uniform flow speed ranging from 10 m/s to 40 m/s. The experimental set-up consisted of a treated NACA 0012 airfoil mounted between two side walls, with a distance of approximately 1 m between the nozzle exit and the airfoil leading edge. Far-field noise was measured using a 73-microphone beamforming array with 9 spiral arms, aligned vertically with the center of the airfoil trailing edge. The far-field sound pressure level (SPL) was calculated as $\mathrm{SPL} = 20\log_{10}(p_{rms}/p_0)$, where p_{rms} represents the root-mean-square sound pressure values for a certain center frequency. These were obtained from the

beamforming array data integrated over one-third octave frequency bands. Given the microphone arrangement used for the present study, the SPL results are most reliable between 600 Hz and 4000 Hz. As an example of a typical far-field sound measurement, the beamforming map of the untreated test configuration for $\alpha_f = 0°$ and a center frequency of 1000 Hz is shown in Fig. 3. Note that the airfoil position is outlined with a black solid line. It can be clearly seen that the array was properly aligned with the trailing edge and that the trailing edge is indeed the prevailing noise source from the airfoil. Far-field noise spectra were obtained by integrating the pressure field over the integration region, enclosed within the dashed lines in Fig. 3. This procedure was repeated for different center frequencies.

Dynamic surface pressure data were sampled at 2^{15} Hz for 24 s and post-processed using Welch's method. In doing so, the surface pressure fluctuation power spectral density Φ_{pp} was obtained for a window size of 2^{12} samples and a Hamming window with 50 % overlap. In the following sections, the surface pressure fluctuation power spectral density, referred to as PSD, will be presented as PSD = $10\log_{10}\left(\Phi_{pp}/p_0^2\right)$. All near-field pressure transducers and far-field beamforming array microphones were calibrated following a procedure already employed in previous studies [15, 17, 38]. Each installed transducer and a G.R.A.S. 40PL reference microphone were simultaneously subjected to white noise produced by a Visaton FRS 8 speaker, such that a transfer function was obtained for each microphone pair. The reference microphone was calibrated using a G.R.A.S. 42AA pistonphone prior to calibrating the other microphones.

Static pressure was measured using the pressure taps on both the pressure and suction side of the airfoil. The signals were transferred to a Chell μDAQ-32DTC Smart Pressure Scanner via polyurethane tubing of about 1 m in length. They were sampled with a rate of 1000 Hz for 60 s and then time-averaged. Boundary layer velocity measurements were performed using constant temperature hot-wire anemometry with a type Dantec 55P15 boundary layer sensor probe. The probe was operated by a Dantec Streamline Pro system with a CTA91C10 module and calibrated using a Dantec 54H10 calibrator. All velocity measurements were sampled at 2^{15} Hz for 16 s, similar to the dynamic pressure measurements.

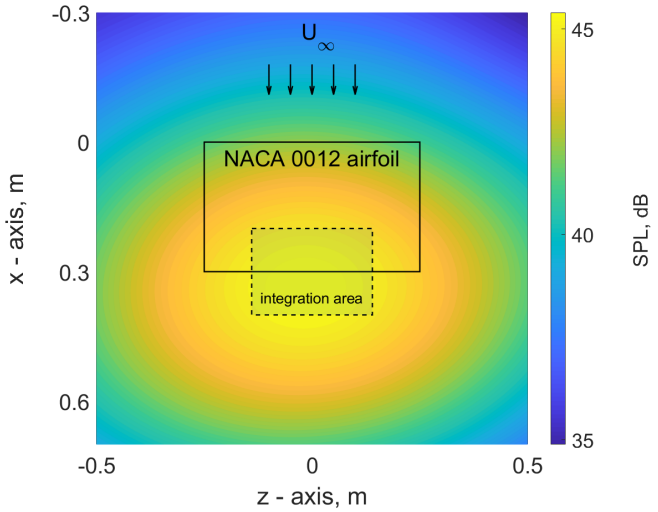

Fig. 3 Beamforming contour map for the NACA 0012 airfoil without finlet treatment at $\alpha_f = 0°$ and a center frequency of 1000 Hz.

IV. Far-Field Analysis

Far-field sound pressure levels measured using the beamforming array provide a direct assessment of the effectiveness of the surface treatments in reducing the airfoil trailing edge noise. Based on the far-field noise data presented in this section, a number of cases will be selected for further near-field analysis. In particular, the results will be used to extract the most crucial parametric settings of the finlet treatments with respect to trailing edge noise reduction. Later, selected configurations will be investigated thoroughly in terms of their near-field flow characteristics and the underlying physics of noise reduction. In order to determine the ranges for the finlet height, h_F, and the angle of attack, α_f, most relevant for further investigations, the effects of varying h_F on the far-field noise are examined for different α_f. Further parameters considered in the discussion are the finlet spacing and position. In the present study, all the finlet treatments have a

length of $l_F = 65$ mm. It should be mentioned that, although care has been taken during the integration of the trailing edge noise, the far-field noise outside the range 600 Hz $< f <$ 4000 Hz still carries comparatively large uncertainties and caution should be exercised when interpreting those results.

A. Effect of Finlet Height

Results for treatments with spacing $s_F = 4$ mm, various finlet heights, h_F, and angles of attack, α_f, applied at $p_F = 0.9c$ are shown in Fig. 4. At each angle of attack, the data for the treated airfoil configurations are plotted next to that for the untreated one, referred to as the baseline. According to Mayer et al. [35], the transition of the NACA 0012 baseline configuration to flow separation and stall occurs at $\alpha_f = 12°$. Thus, the flow over the airfoil remains attached in the test range of $0° \leqslant \alpha_f \leqslant 8°$, which represents the normal operating mode of an airfoil. A clear trend in trailing edge noise reduction can be observed as h_F is varied from 2 mm to 6 mm within the considered range of α_f. In general, the treatments with heights lower than $h_F = 6$ mm showed a smaller far-field noise reduction throughout the considered frequency range, except for high frequencies around 5000 Hz. Further increasing the finlet height to $h_F = 8$ mm, the trend is no longer followed. Instead, the noise reduction efficiency only improves up to 2000 Hz, whereas for frequencies exceeding this value the finlets with $h_F = 8$ mm were outperformed by the finlets with $h_F = 6$ mm. With increasing angle of attack, the highest finlets showed improved noise reduction capability compared to the lower finlets and, in terms of the frequency range where the SPL is reduced compared to the baseline, also to themselves. Since the boundary layer thickness at the trailing edge is expected to increase with α_f, there appears to be a correlation between the ratio h_F/δ and the trailing edge noise reduction by the finlet treatments. At $\alpha_f = 8°$, the treatment with $h_F = 8$ mm caused a reduction in SPL across the whole frequency range. Also, it can be observed in Fig. 4d that the treatment with $h_F = 6$ mm seems to decrease the far-field sound at frequencies higher than 4000 Hz more efficiently than any of the other treatments. For the discussion of the underlying noise reduction mechanisms, more detailed information about the

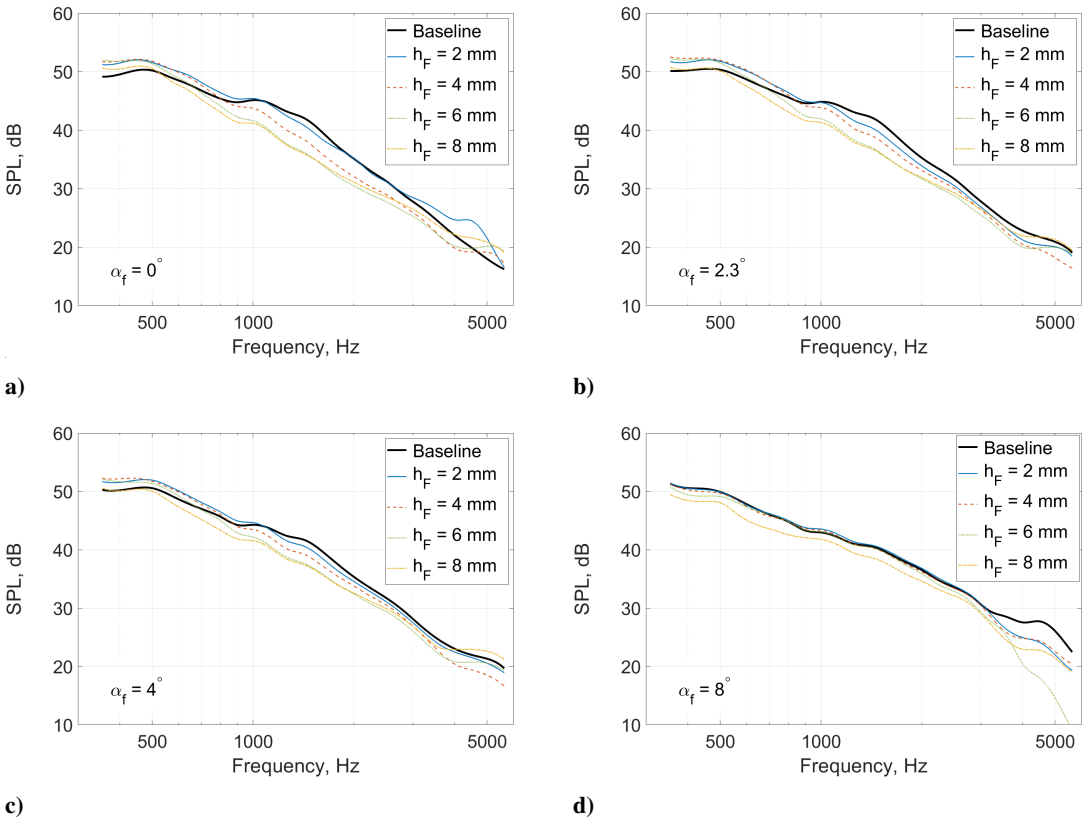

Fig. 4 Far-field SPL for finlets at $p_F = 0.9c$, with $s_F = 4$ mm, and different finlet heights at $Re_c = 4 \cdot 10^5$: a) $\alpha_f = 0°$, b) $\alpha_f = 2.3°$, c) $\alpha_f = 4°$, and d) $\alpha_f = 8°$.

boundary layer at different angles of attack is needed. From the the far-field noise results, it can be said that, within the range of $\alpha_f = 0°$ to $\alpha_f = 4°$, the different treatments considered show similar noise reduction potentials compared to the baseline and a decrease of the noise radiated into the far-field as the finlet height increases from $h_F = 2\,\text{mm}$ to $h_F = 6\,\text{mm}$. The cases $h_F = 4\,\text{mm}$, $h_F = 6\,\text{mm}$ and $h_F = 8\,\text{mm}$ at $\alpha_f = 0°$ are chosen for a discussion of near-field data in Secion V.A.

B. Effect of Finlet Spacing

The effects of finlet spacing on the far-field noise are illustrated in Fig. 5. Two finlet spacings were considered here, $s_F = 4\,\text{mm}$ and $s_F = 6\,\text{mm}$, where the finlet height was kept constant at $h_F = 6\,\text{mm}$ and the finlet position was $p_F = 0.9c$. For a flat plate, the ideal finlet spacing was found to be somewhere in the range of $s_F = 4\,\text{mm}$ to $s_F = 6\,\text{mm}$, independent of the chord-based Reynolds number, at least within a range of $3.87 \cdot 10^5 \leq Re_c \leq 7.7 \cdot 10^5$ [27]. The same was found to be valid for a DU96-W180 airfoil in a region of $2.5 \cdot 10^6 \leq Re_c \leq 3 \cdot 10^6$ [25]. Thus, a similar spacing range is chosen for the tests in the present study. A reduction in the far-field SPL was observed for both cases above 700 Hz at $\alpha_f < 8°$. As can be seen in Figs. 5a - c, an increase of s_F led to a smaller reduction between 700 Hz and 4000 Hz for $\alpha_f < 8°$. Considering only the mid-frequency range of 600 Hz to 4000 Hz, where measurements are most reliable, it can be said that from the two different treatments, the one with the smaller spacing seems to result in more dominant noise reduction. In the case of $\alpha_f = 8°$, shown in Fig. 5d, both treatments lost their ability to reduce far-field noise in the mid-frequency range.

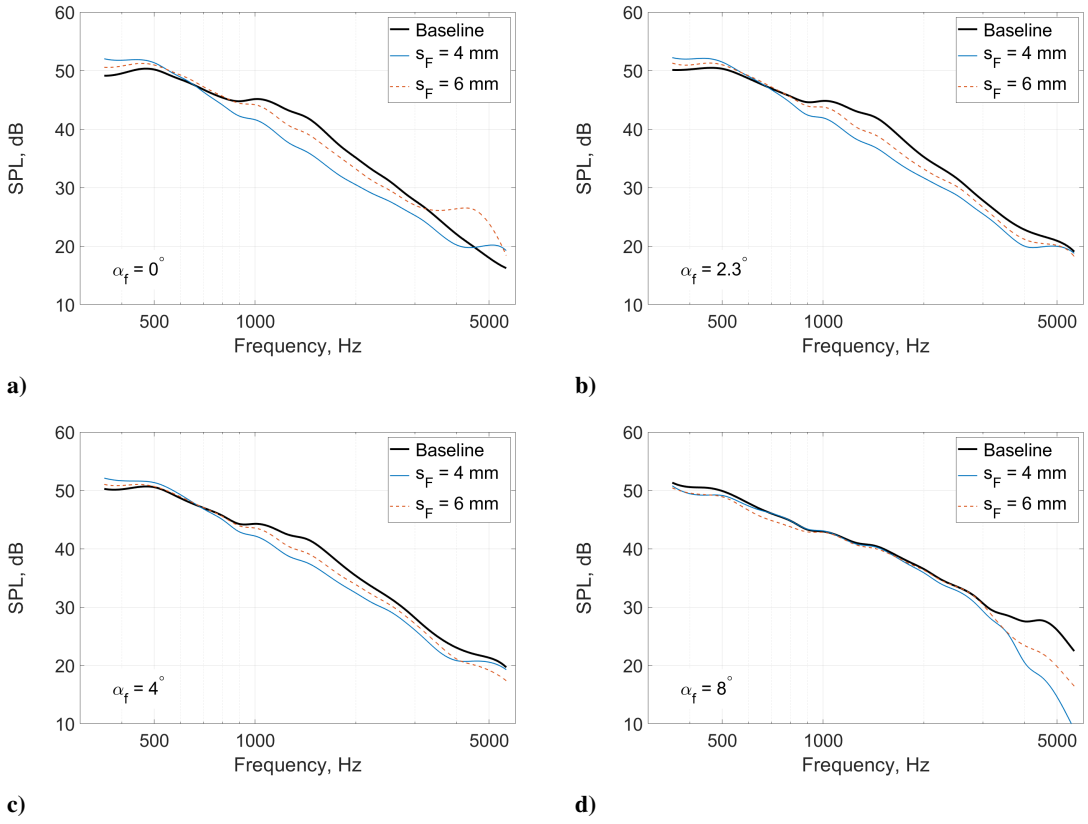

Fig. 5 Far-field SPL for finlets at $p_F = 0.9c$, with $h_F = 6\,\text{mm}$, and different spacings at $Re_c = 4 \cdot 10^5$: a) $\alpha_f = 0°$, b) $\alpha_f = 2.3°$, c) $\alpha_f = 4°$, and d) $\alpha_f = 8°$.

C. Effect of Finlet Position

Clark et al. [25] demonstrated that finlets can affect the boundary layer turbulence as it approaches the trailing edge. Nevertheless, it remains unclear for the case of an airfoil whether the finlets should be applied at the trailing edge or at some distance upstream to achieve maximum far-field noise reduction. The present study investigates whether moving the finlets upstream of the trailing edge of the airfoil yields further benefits to the far-field noise reduction, in comparison to the finlets being applied at the trailing edge itself. Thus, in this section, the changes to the far-field noise levels are investigated as the finlet position, p_F, is varied. For this, the parameters other than p_F were kept fixed at $h_F = 6\,\text{mm}$, $s_F = 4\,\text{mm}$ and $l_F = 65\,\text{mm}$. The results for four different positions at various angles of attack, α_f, are depicted in Fig. 6. It can be clearly observed that there is a continuous increase of noise reduction efficiency as the finlet position moves closer to the trailing edge up to $p_F = 0.9c$. The configuration for which the treatment was installed flush to the trailing edge performed most effectively for frequencies below 1500 Hz. Although the SPL was reduced across the entire frequency range considered, the configuration with $p_F = 1.0c$ turned out to be slightly less effevtive than the configuration with $p_F = 0.9c$ for frequencies between 1500 Hz and 4500 Hz. The intersection of the results for the two different finlets could indicate a change of the prevailing noise reduction mechanism. If the large-scale turbulent structures, associated with the lower frequencies, were lifted away from the trailing edge by finlets installed flush to the trailing edge as postulated by [28, 29], this could explain the reduction at low frequencies up to 1500 Hz, whereas the lower far-field SPL for $p_F = 0.9c$ at higher frequencies suggests that those smaller structures tend to be less energetic after leaving the treatment. Further insight into the physics will be given by the near-field data, which will be discussed in Section V.

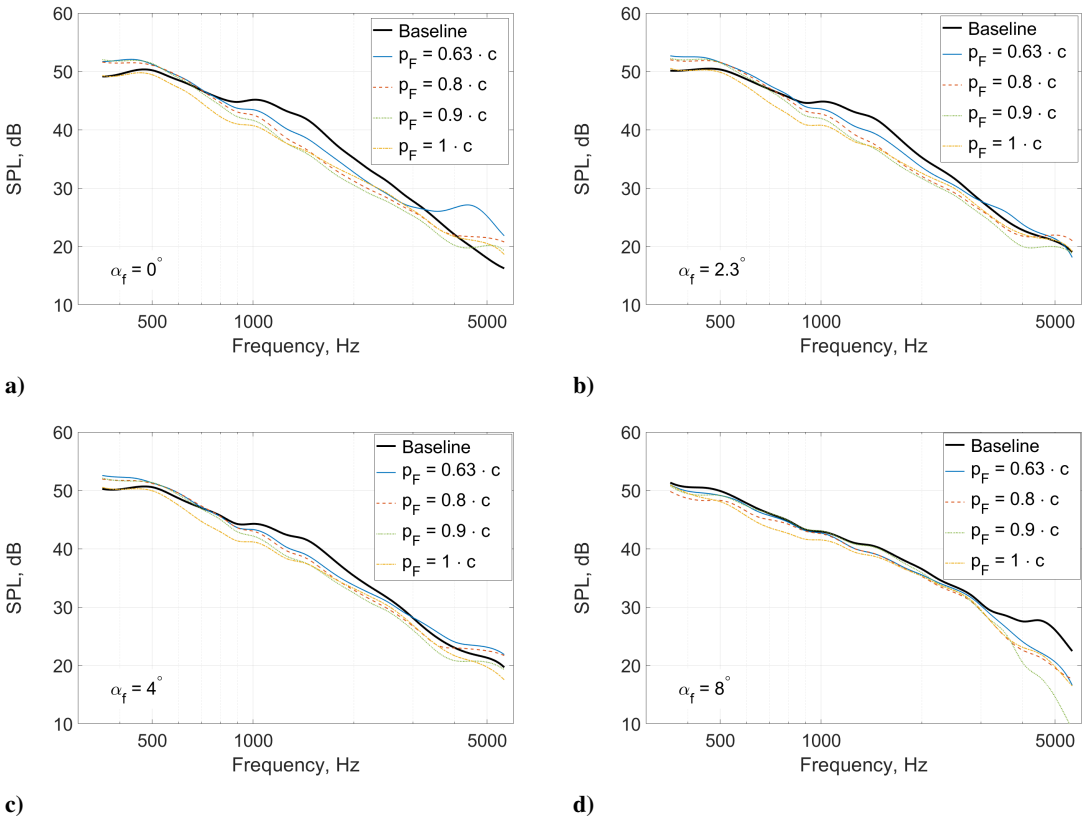

Fig. 6 Far-field SPL for finlets with $h_F = 6\,\text{mm}$, and $s_F = 4\,\text{mm}$ at different positions at $Re_c = 4 \cdot 10^5$: a) $\alpha_f = 0°$, b) $\alpha_f = 2.3°$, c) $\alpha_f = 4°$, and d) $\alpha_f = 8°$.

V. Near-Field Analysis

Far-field data are important to evaluate the actual capability of the finlet treatments to reduce trailing edge noise. To analyze and determine the underlying noise reduction mechanism, the knowledge on the near-field surface pressure and velocity fluctuations becomes necessary. In this section, we attempted to explain the physics that lead to the decreased SPL when surface treatments are applied. Therefore, data measured in the near-field, i.e. surface pressure and boundary layer velocity, are used. Amiet [8] argued that the far-field sound power spectral density depends on the spanwise correlation length of turbulence structures $\Lambda_z(f)$ and the surface pressure fluctuation PSD $\Phi_{pp}(f)$ at the trailing edge. Thus, these are important quantities to be examined in the context of this study. Additionally, the static pressure distribution on the airfoil was investigated, as it contains essential information on the time-averaged flow characteristics.

A. Effect of Finlet Height

From the far-field data, it was found that the finlets achieved better noise reduction as the finlet height, h_F, was increased from 2 mm to 6 mm. Further increasing h_F, however, resulted in a rise of the SPL at high frequencies rather than causing any further overall noise reduction. Figure 7 shows the boundary layer thickness measured at the trailing edge at the two different corrected angles of attack of 0° and 4°, respectively. The boundary layer thickness was determined as the distance from the airfoil surface along the y-axis where the streamwise velocity, u, reached an absolute value of $0.99U_e$. Here, U_e is the velocity measured in a distance far above the airfoil surface, to ensure that it reflects the free-stream velocity. For the sake of simplicity, the origin of the y-axis has been shifted from the airfoil center line to the airfoil surface for the presentation of the boundary layer thickness. As can be seen from Fig. 7, a height variation between $h_F = 2$ mm and $h_F = 8$ mm corresponded to a ratio of finlet height to boundary layer thickness of $h_F/\delta = 0.17$ at $\alpha_f = 4°$ for the lowest treatment and $h_F/\delta = 0.78$ at $\alpha_f = 0°$ for the finlets with $h_F = 8$ mm (i.e. the boundary layer thickness, δ, at $\alpha_f = 4°$ and $\alpha_f = 0°$ are 11.5 mm and 10.2 mm, respectively). These values cover the range of finlet heights ($h_F/\delta = 0.25$ to 0.8) suggested by Clark et al. [25] and Afshari et al. [27].

In Fig. 8, the surface pressure fluctuation PSD is shown for treatments with different finlet heights, h_F, and a spacing $s_F = 4$ mm at $p_F = 0.9c$ and $\alpha_f = 0°$. The development of the PSD as the turbulence leaves the treatment and approaches the trailing edge is illustrated by presenting the results at two selected downstream pressure measurement locations. These are indicated by a black line in the drawing of the finlets applied on the NACA 0012 airfoil added to each plot. The trend very well reflects some previous findings from the far-field observations. Close to the trailing edge at $x/c = 0.99$, the PSD for all treatments is elevated to some extent for frequencies lower than 1000 Hz. It is therefore inferred that the finlets give rise to large flow structures in their wake such as a separation zone at the end of the finlets or a shear layer resulting from a lifting effect due to the treatments. As reported by Afshari et al. [27], an increase in low frequency related to a shear layer on top of the treatments can be attributed to vortex shedding at the

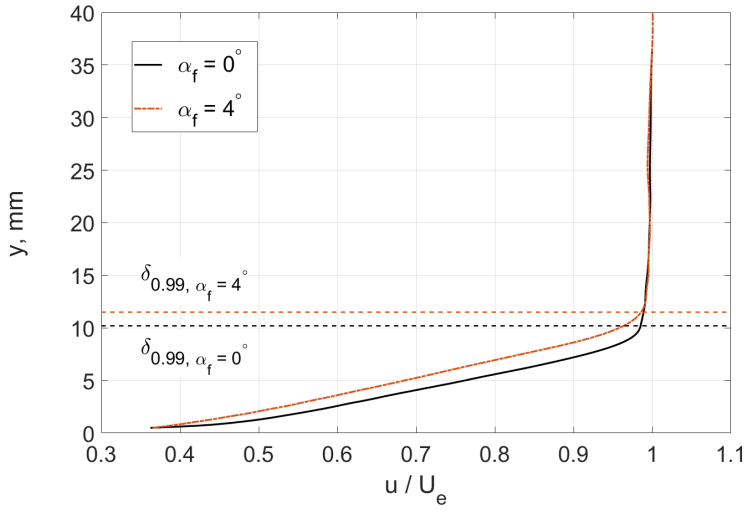

Fig. 7 Boundary layer thickness measured at the trailing edge of the untreated airfoil at $Re_c = 4 \cdot 10^5$, $\alpha_f = 0°$ and $\alpha_f = 4°$, respectively.

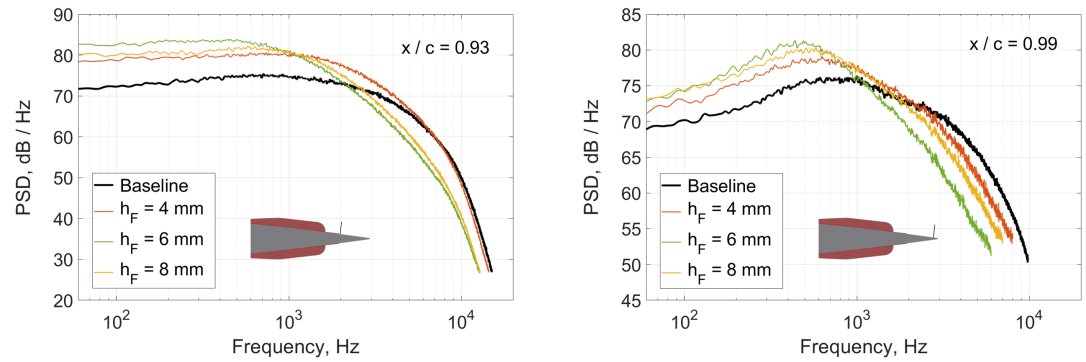

a) b)

Fig. 8 Surface pressure fluctuation PSD for finlets at $p_F = 0.9c$, with $s_F = 4\,\text{mm}$ and different heights at $Re_c = 4 \cdot 10^5$ and $\alpha_f = 0°$: a) $x/c = 0.93$ and b) $x/c = 0.99$.

finlet trailing edge, as it is the case for a backward facing step. The elevation in the low frequency range is smallest for the $h_F = 4\,\text{mm}$ case, and largest for the finlets with $h_F = 6\,\text{mm}$. Interestingly, a point of intersection seems to exist, where the finlet effectiveness is reversed. As can be seen from Figs. 8a and b, the point of intersection moves from approximately 1000 Hz to somewhere around 800 Hz as the measurement position moves downstream from finlet exit to the trailing edge. For frequencies higher than the intersection frequency, the treatment causing the highest elevation at low frequencies produces the largest reduction of surface pressure fluctuations. The fact that the surface pressure PSD of the finlet treatment with $h_F = 8\,\text{mm}$ lies in between that of the finlet treatments with $h_F = 4\,\text{mm}$ and $h_F = 6\,\text{mm}$ indicates that there possibly exists an optimal h_F/δ ratio. Under the present experimental conditions, this was determined to be approximately at $h_F/\delta = 0.6$. The noise reduction becomes less effective below and above this optimal ratio.

B. Effect of Finlet Spacing

Prior research has shown that the finlet spacing, s_F, is one of the most important parameters affecting the noise reduction capability of the finlets. According to Afshari et al. [27] the flow through the finlets on a flat plate experiences

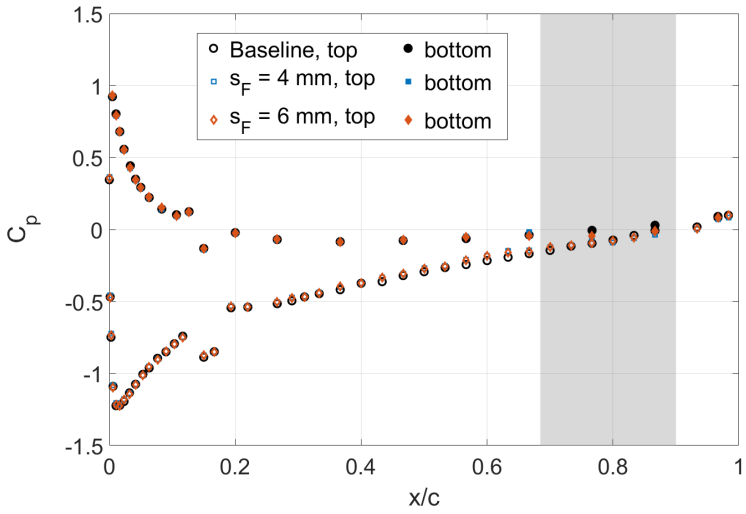

Fig. 9 Pressure coefficient for finlets at $p_F = 0.9c$, with $h_F = 6\,\text{mm}$ and different spacings at $Re_c = 4 \cdot 10^5$ and $\alpha_f = 4°$.

strong channeling effects when s_F exceeds a certain threshold. This means that instead of being pushed upward and relocated along the y_F-axis, similar to the case of a solid step with the profile of the finlet, the flow follows the channels formed by the finlet walls and is thus subject to increased friction induced by wall surfaces. As a result, flow energy contained in the turbulent structures within the boundary layer is dissipated. To find out whether this scenario is also a plausible explanation for the noise reduction due to finlets on the NACA 0012 airfoil confirmed by the beamforming results in Section IV, the effects of varying s_F on the boundary layer characteristics were investigated. Figure 9 shows the distribution of pressure coefficients, C_p, on the suction (or top) and the pressure (or bottom) sides of the airfoil at $\alpha_f = 4°$. Here, finlet treatments with height $h_F = 6\,\text{mm}$ and distinct s_F applied at $p_F = 0.9c$ are compared to each other and the baseline configuration. Looking at the baseline case, the effects of the tripping can be seen on both the pressure and suction side at $x/c = 0.12$. In the treated area indicated with a grey band, slight reductions of the static pressure can be observed on both the suction and the pressure sides. On the suction side, these follow a small increase upstream of the finlets. Before further discussing these observations, it should be noted that the overall change of the static pressure distribution around the airfoil is very small. There are no significant changes in the pressure gradient and thus, no extensive flow changes are expected. In particular, the data suggest that the finlets do not particularly alter the aerodynamic performance of the airfoil. Nevertheless, the slight increase in pressure upstream of the treatments indicates a marginal deceleration of the flow. Inside of the treated area, the pressure decrease points to two possible events. One is that the flow was accelerated within the finlet treatment area and the pressure was reduced as a result of the increased velocity considering Bernoulli's equation for fricitonless, stationary and incompressible flows. Another possiblity is that the boundary layer separated and the mean flow was lifted away from the surface, causing a reduction of static pressure compared to the baseline within the separation region. Furthermore, no remarkable changes due to the varied finlet spacing can be identified in Fig. 9.

The evolution of the dynamic pressure along the chord on the suction side of the airfoil and through finlet treatments with different spacings is illustrated in Fig. 10. Each measurement position considered is indicated with a black line on a drawing of the finlet treatment applied on the airfoil as in the previous section. Upstream of the treatments, there are no major changes in the surface pressure fluctuation PSD, Φ_{pp}, as can be seen in Fig. 10a. According to Figs. 10b to c, Φ_{pp} rose over a range of frequencies up to $f = 1000\,\text{Hz}$ in between of the finlets. For the treatment with $s_F = 4\,\text{mm}$ the increase in the surface pressure flucuation PSD in this frequency range is higher than for $s_F = 6\,\text{mm}$. Downstream of the finlets, Φ_{pp} was reduced at frequencies higher than 1000 Hz, whereas the elevation at low frequencies remained. Again, just as in the case of different heights, a point of intersection can be identified, beyond which the efficiency of the treatment with the smallest spacing surpasses the other cases. Toward the trailing edge, the reduction at high frequencies strengthens further, whereas the low-frequency increase remains comparable to the measurement position right after the finlets. The observed results suggest that the presence of a treatment on the suction side of an airfoil leads to the production of large flow structures. These appear as the flow enters the finlets and, in the case of an airfoil, stretch out toward the trailing edge. Their presence is likely to lead to a reduction of high-frequency fluctuations of the dynamic pressure, probably by lifting smaller flow structures away from the surface, as Bodling and Sharma [28, 29] suggested. The lifting effect could be beneficial in terms of noise reduction by preventing high-frequency turbulence structures being convected past the trailing edge. Besides a detachment of small eddies from the airfoil surface, the presence of a treatment may also lead to a slight shift of the separation point upstream of the trailing edge. Considering an earlier detachment of even the larger low-frequency turbulence structures at high angles of attack, this could also explain the increased far-field noise reduction frequency range at $\alpha_f = 8°$ discussed in Section IV.

Before the effects of a variation of p_F are discussed, the role of the spanwise correlation length of boundary layer turbulence structures, Λ_z, for the noise reduction has to be elucidated. According to Amiet's theory, besides Φ_{pp}, Λ_z is an important near-field flow feature governing the trailing edge noise. As can be seen in Fig. 11, Λ_z undergoes no significant changes across the entire frequency range and thus is expected to contribute very little toward the overall changes in the sound pressure level in this case. The lack of an increase in the lateral correlation length at frequencies lower than 1000 Hz suggests that the structures forming at the finlet leading edges were mainly oriented across the x-y plane. Thus, the structures are not likely to be reflected by the results for the spanwise correlation length.

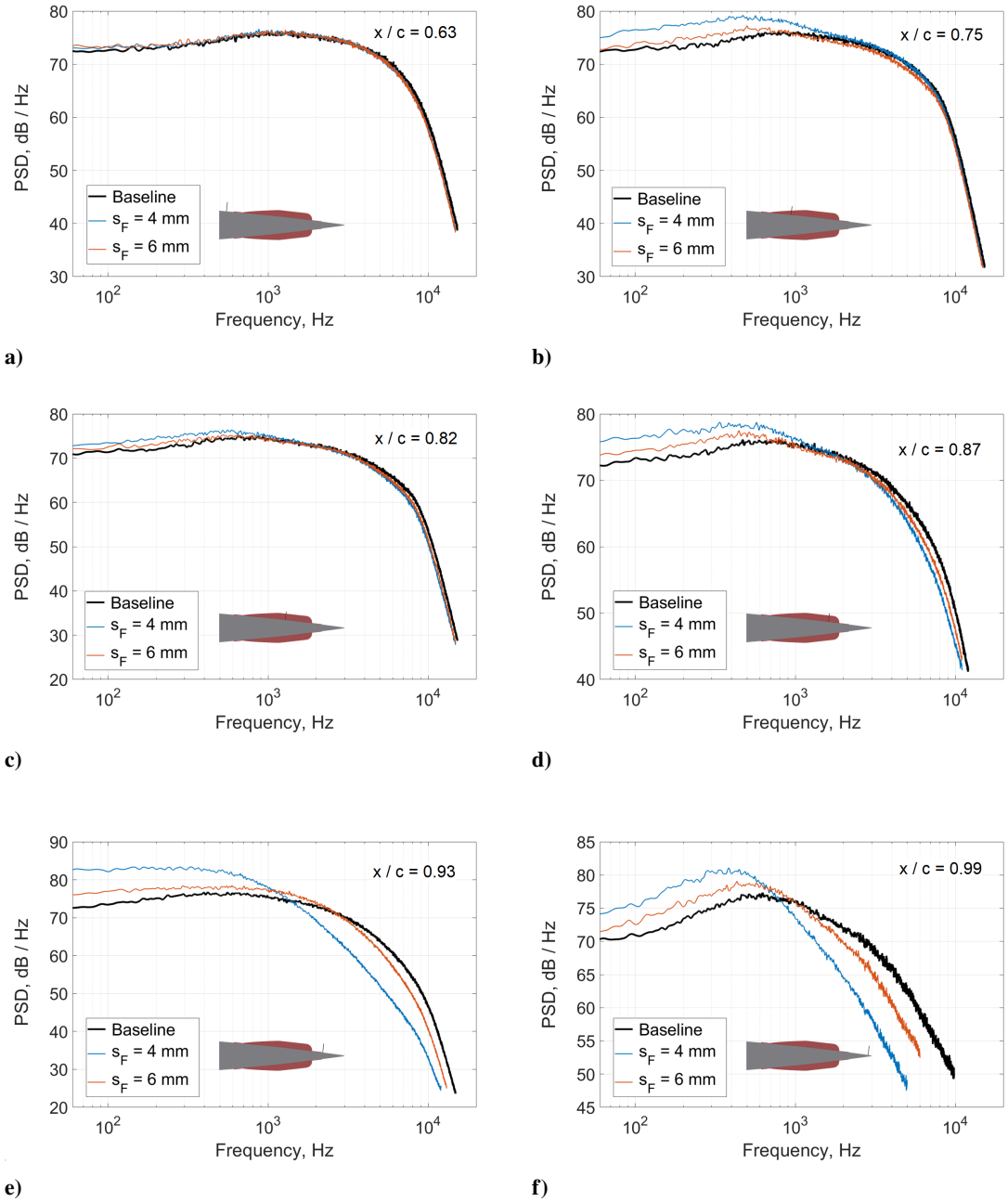

Fig. 10 Surface pressure fluctuation PSD for finlets at $p_F = 0.9c$, with $h_F = 6$ mm, and different spacings at $Re_c = 4 \cdot 10^5$ and $\alpha_f = 4°$: a) $x/c = 0.63$, b) $x/c = 0.75$, c) $x/c = 0.82$, d) $x/c = 0.87$, e) $x/c = 0.93$ and f) $x/c = 0.99$.

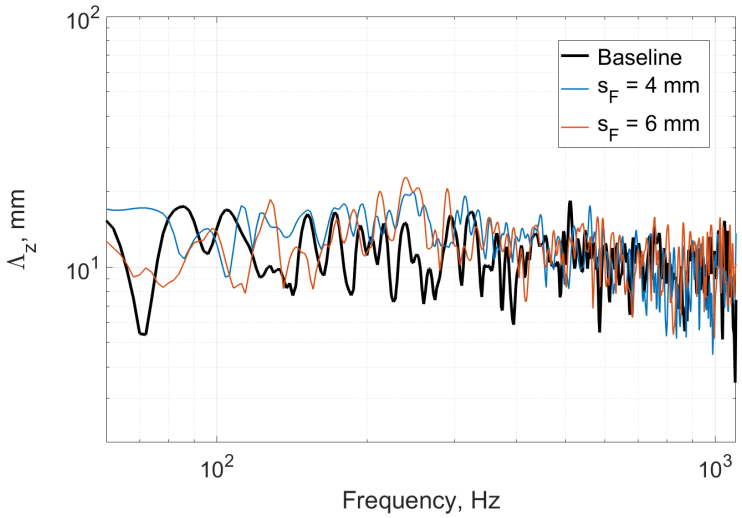

Fig. 11 Spanwise correlation length of the boundary layer turbulence structures at $x/c = 0.99$ for finlets at $p_F = 0.9c$, with $h_F = 6$ mm, and different spacings at $Re_c = 4 \cdot 10^5$ and $\alpha_f = 4°$.

C. Effect of Finlet Position

A particular focus of the present finlet studies is set on how the treatments affect the turbulence structures approaching the trailing edge. It is believed that the examination of the finlet wake and its development provides further insights into the role of these turbulence structures. Figure 12 shows the development of the surface pressure fluctuation PSD, Φ_{pp}, as the flow passed treatments with $h_F = 6$ mm and $s_F = 4$ mm. One treatment was installed flush with the trailing edge, the other two finlet positions investigated are further upstream at $p_F = 0.9c$ and $p_F = 0.63c$, consistent with those considered for the far-field studies. The flushed mounted finlet will be referred to as trailing edge (TE) treatment. As expected, the development of the dynamic pressure along the finlet length remains similar for each case. Since the trailing edge noise is mostly related to the boundary layer characteristics at the trailing edge, the measurement position represented by Fig. 12d is most relevant. Both of the upstream treatments produced an elevation of Φ_{pp} at frequencies lower than 700 Hz, which explains the increase in the far-field SPL in that frequency region. At higher frequencies, those treatments caused a reduction of both far-field noise and Φ_{pp}. In the case of the TE treatment, the turbulent structures likely remained between the finlets until they were convected past the trailing edge. Thus, it seems that there was no time for large-scale structures to develop, leading to no SPL rise at low frequencies, but also to a less efficient lifting effect, i.e. small-scale eddies likely remained closer to the flat plate surface and thus there was no decrease of the surface pressure fluctuation PSD at frequencies higher than 1000 Hz. Studying the development of Φ_{pp} for all different treatment positions, it can be observed that in each case a rise at low frequencies emerged and was sustained until past the trailing edge. This indicates, that the presence of a treatment on the NACA 0012 airfoil generally produced some large-scale turbulent structures, which then lifted smaller turbulence structures from the wall. As already described by Bodling and Sharma [28, 29], the detachment of small structures from the airfoil surface results in far-field noise reduction, since they are lifted away from the surface and thus prevented from interacting with the trailing edge when convecting past it.

As can be seen from the development of the dynamic pressure for $p_F = 0.9c$ in Fig. 12, the main reduction of Φ_{pp} at frequencies above 1000 Hz only set in once the flow had left the finlets. Following the development of Φ_{pp} from the end of the finlet treatment applied closest to the leading edge toward the trailing edge shows an interesting feature. Along the distance considered, the decrease at high frequencies continues. Therefore, it can be inferred that it takes some time for the related effect to be fully deployed. This is probably the reason why the treatment applied at $p_F = 1.0c$ did not show any reduction at high frequencies. However, the case of $p_F = 0.9c$ still showed better results at the trailing edge than that of $p_F = 0.63c$, which may be due to the more convenient degree of the airfoil profile curvature at that position. It is thus assumed that it takes some distance to allow the larger structures to develop and the smaller eddies to become fully detached or dissipated, which is corroborated by the fact that the most efficient noise reduction is observed at $p_F = 0.9c$.

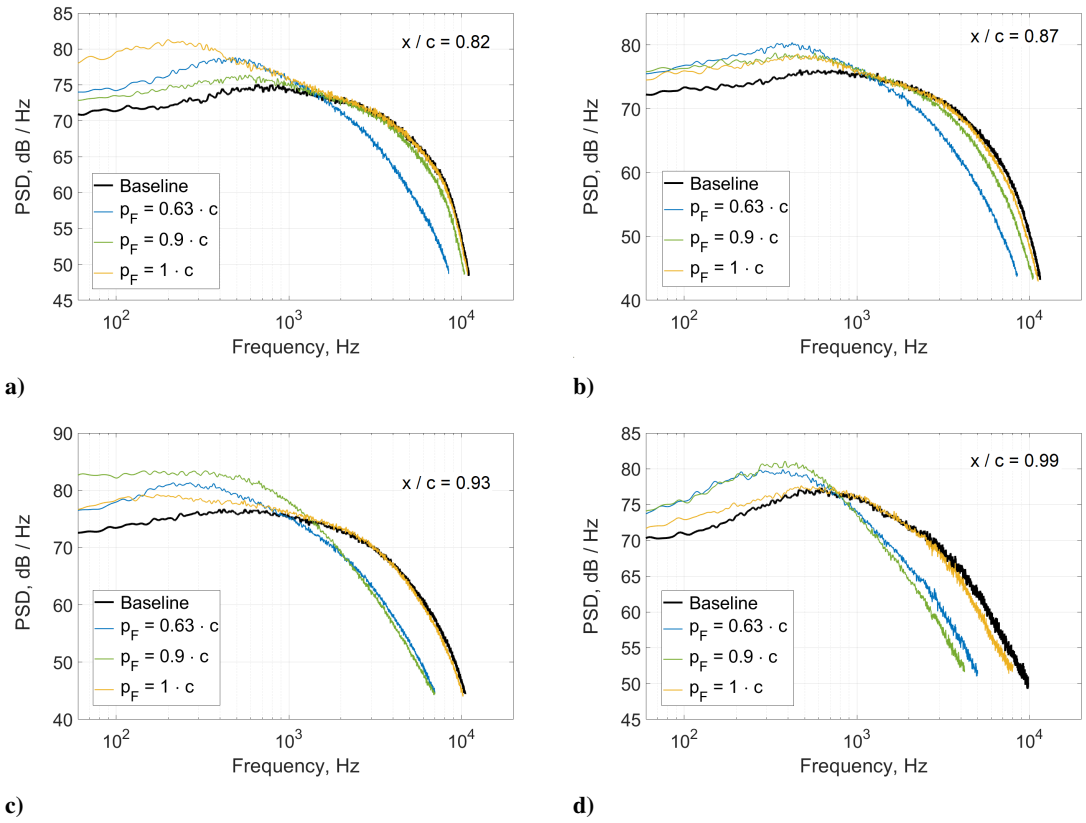

Fig. 12 Surface pressure fluctuation PSD for finlets with $h_F = 6\,\text{mm}$, $s_F = 4\,\text{mm}$, at different positions, p_F, $Re_c = 4 \cdot 10^5$ and $\alpha_f = 4°$: a) $x/c = 0.82$ (within the two rear treatments), b) $x/c = 0.87$ (within the two rear treatments), c) $x/c = 0.93$ (within the TE treatment, downstream of the others) and d) $x/c = 0.99$ (at the trailing edge).

VI. Conclusions and Future Work

Finlet treatments were applied on a NACA 0012 airfoil to investigate their capability of trailing edge noise reduction and identify the related mechanisms. Their design follows that of Afshari et al. [26, 27], such that a comparison with finlet application on a flat plate is possible. It was found that for the configurations of this study, the occurrence of an eddie-detachment effect is most likely responsible for the trailing edge noise reduction. The addressed detachment process of eddies from the airfoil surface was examined using data measured along the path of the flow and particularly in between of the finlets. Comparing this data to the far-field SPL, it was concluded that the decrease in small-scale turbulent structures close to the wall leads to a reduction of trailing edge noise. The decrease is correlated to an increase of dynamic pressure fluctuations at frequencies lower than 1000 Hz, which indicates that the small-scale turbulent structures were lifted away from the surface due to the presence of larger structures. Further, it was found that the reduction in the surface pressure PSD at frequencies above 1000 Hz attained its maximum efficiency somewhere in the wake of the finlets. Thus, the optimal application area for efficient noise reduction is not necessarily right at the trailing edge. It was shown that the treatment efficiency is also dependent of the ratio of finlet height to boundary layer thickness, and thus of the angle of attack. Hence, it remains the task of end users to identify the critical configurations and choose finlet parameter sets accordingly.

Acknowledgments

The first author appreciates the financial support of the EU H2020 ARTEM project under the grant agreement ID 769359.

References

[1] Macaraeg, M. G., "Fundamental investigations of airframe noise," *4th AIAA/CEAS Aeroacoustics Conference*, 1998, pp. 123–132.

[2] Lilley, G. M., "The prediction of air frame noise and comparison with experiment," *Journal of Sound and Vibration*, Vol. 239, No. 4, 2001, pp. 849–859.

[3] Dobrzynski, W., "Almost 40 years of airframe noise research: what did we achieve?" *Journal of aircraft*, Vol. 47, No. 2, 2010, pp. 353–367.

[4] Huss, A., Spoerri, A., Egger, M., and Röösli, M., "Aircraft noise, air pollution, and mortality from myocardial infarction," *Epidemiology*, Vol. 21, No. 6, 2010, pp. 829–836.

[5] Nissenbaum, M. A., Aramini, J. J., and Hanning, C. D., "Effects of industrial wind turbine noise on sleep and health," *Noise and Health*, Vol. 14, No. 60, 2012, pp. 237–243.

[6] Lockard, D. P., and Lilley, G. M., "The airframe noise reduction challenge," Tech. mem. tm–2004–213013, NASA, Langley Research Center, Hampton, Virginia, 2004.

[7] Amiet, R. K., "Acoustic radiation from an airfoil in a turbulent stream," *Journal of Sound and Vibration*, Vol. 41, No. 4, 1975, pp. 407–420.

[8] Amiet, R. K., "Noise due to turbulent flow past a trailing edge," *Journal of Sound and Vibration*, Vol. 47, No. 3, 1976, pp. 387–393.

[9] Roger, M., and Moreau, S., "Back-scattering correction and further extensions of Amiet's trailing-edge noise model. Part 1: Theory," *Journal of Sound and Vibration*, Vol. 286, No. 3, 2005, pp. 477–506.

[10] Azarpeyvand, M., Gruber, M., and Joseph, P. F., "An analytical investigation of trailing edge noise reduction using novel serrations," *19th AIAA/CEAS Aeroacoustics Conference*, 2013.

[11] Mayer, Y. D., Lyu, B., Jawahar, H. K., and Azarpeyvand, M., "Toward a semi-empirical noise prediction for airfoils with serrated trailing edges," *AIAA/CEAS Aeroacoustics Conference*, 2018.

[12] Chong, T. P., and Vathylakis, A., "On the aeroacoustic and flow structures developed on a flat plate with a serrated sawtooth trailing edge," *Journal of Sound and Vibration*, Vol. 354, 2015, pp. 65–90.

[13] Mayer, Y. D., Lyu, B., Jawahar, H. K., and Azarpeyvand, M., "A semi-analytical noise prediction model for airfoils with serrated trailing edges," *Renewable Energy*, Vol. 143, 2019, pp. 679–691.

[14] Wolf, A., Lutz, T., Würz, W., Krämer, E., Stalnov, O., and Seifert, A., "Trailing edge noise reduction of wind turbine blades by active flow control," *Wind Energy*, Vol. 18, No. 5, 2015, pp. 909–923.

[15] Szoke, M., Fiscaletti, D., and Azarpeyvand, M., "Effect of inclined transverse jets on trailing-edge noise generation," *Physics of Fluids*, Vol. 30, No. 8, 2018.

[16] Geyer, T., Sarradj, E., and Fritzsche, C., "Measurement of the noise generation at the trailing edge of porous airfoils," *Experiments in Fluids*, Vol. 48, No. 2, 2010, pp. 291–308.

[17] Ali, S. A. S., Azarpeyvand, M., and Da Silva, C. R. I., "Trailing-edge flow and noise control using porous treatments," *Journal of Fluid Mechanics*, Vol. 850, 2018, pp. 83–119.

[18] Showkat Ali, S. A., Azarpeyvand, M., Szoke, M., and Ilário Da Silva, C. R., "Boundary layer flow interaction with a permeable wall," *Physics of Fluids*, Vol. 30, No. 8, 2018.

[19] Ai, Q., Azarpeyvand, M., Lachenal, X., and Weaver, P. M., "Aerodynamic and aeroacoustic performance of airfoils with morphing structures," *Wind Energy*, Vol. 19, No. 7, 2016, pp. 1325–1339.

[20] Kamliya Jawahar, H., Ai, Q., and Azarpeyvand, M., "Experimental and numerical investigation of aerodynamic performance for airfoils with morphed trailing edges," *Renewable Energy*, Vol. 127, 2018, pp. 355–367.

[21] Afshari, A., Dehghan, A. A., and Azarpeyvand, M., "Novel three-dimensional surface treatments for trailing-edge noise reduction," *AIAA Journal*, Vol. 57, No. 10, 2019, pp. 4527–4535.

[22] Herr, M., and Dobrzynski, W., "Experimental investigations in low-noise trailing-edge design," *AIAA Journal*, Vol. 43, No. 6, 2005, pp. 1167–1175.

[23] Lilley, G. M., "A study of the silent flight of the owl," *4th AIAA/CEAS Aeroacoustics Conference*, 1998.

[24] Clark, I. A., Devenport, W., Jaworski, J. W., Daly, C., Peake, N., and Glegg, S., "The noise generating and suppressing characteristics of bio-inspired rough surfaces," *20th AIAA/CEAS Aeroacoustics Conference*, 2014.

[25] Clark, I. A., Alexander, W. N., Devenport, W., Glegg, S., Jaworski, J. W., Daly, C., and Peake, N., "Bioinspired trailing-edge noise control," *AIAA Journal*, Vol. 55, No. 3, 2017, pp. 740–754.

[26] Afshari, A., Azarpeyvand, M., Dehghan, A. A., and Szőke, M., "Effects of streamwise surface treatments on trailing edge noise reduction," *23rd AIAA/CEAS Aeroacoustics Conference*, 2017.

[27] Afshari, A., Azarpeyvand, M., Dehghan, A. A., Szöke, M., and Maryami, R., "Trailing-edge flow manipulation using streamwise finlets," *Journal of Fluid Mechanics*, Vol. 870, 2019, pp. 617–650.

[28] Bodling, A., and Sharma, A., "Numerical investigation of low-noise airfoils inspired by the down coat of owls," *Bioinspiration and Biomimetics*, Vol. 14, No. 1, 2019.

[29] Bodling, A., and Sharma, A., "Numerical investigation of noise reduction mechanisms in a bio-inspired airfoil," *Journal of Sound and Vibration*, Vol. 453, 2019, pp. 314–327.

[30] Brooks, T. F., Marcolini, M. A., and Pope, D. S., "Airfoil trailing edge flow measurements and comparisons with theory, incorporating open wind tunnel corrections." *AIAA Paper*, 1984.

[31] Garcia Sagrado, A. P., "Boundary layer and trailing edge noise sources," Ph.D. thesis, University of Cambridge, 2008.

[32] Hutcheson, F. V., and Brooks, T. F., "Effects of angle of attack and velocity on trailing edge noise determined using microphone array measurements," *International Journal of Aeroacoustics*, Vol. 5, No. 1, 2006, pp. 39–66.

[33] Gravante, S. P., Naguib, A. M., Wark, C. E., and Nagib, H. M., "Characterization of the pressure fluctuations under a fully developed turbulent boundary layer," *AIAA Journal*, Vol. 36, No. 10, 1998, pp. 1808–1816.

[34] Elsahhar, W., Showkat Ali, S. A., Theunissen, R., and Azarpeyvand, M., "An experimental investigation of the effect of bluff body bluntness factor on wake-vortex noise generation," *AIAA/CEAS Aeroacoustics Conference*, 2018.

[35] Mayer, Y. D., Zang, B., and Azarpeyvand, M., "Aeroacoustic characteristics of a NACA 0012 airfoil for attached and stalled flow conditions," *25th AIAA/CEAS Aeroacoustics Conference*, 2019.

[36] Zang, B., Mayer, Y. D., and Azarpeyvand, M., "An experimental investigation on the mechanism of tollmien-schlichting waves for a naca 0012 aerofoil," *25th AIAA/CEAS Aeroacoustics Conference*, 2019.

[37] Mayer, Y. D., Jawahar, H. K., Szőke, M., Ali, S. A. S., and Azarpeyvand, M., "Design and performance of an aeroacoustic wind tunnel facility at the University of Bristol," *Applied Acoustics*, Vol. 155, 2019, pp. 358–370.

[38] Garcia-Sagrado, A., and Hynes, T., "Wall pressure sources near an airfoil trailing edge under turbulent boundary layers," *Journal of Fluids and Structures*, Vol. 30, 2012, pp. 3–34.